

Tomography of epidermal growth factor receptor binding to fluorescent Affibody *in vivo* studied with magnetic resonance guided fluorescence recovery in varying orthotopic glioma sizes

Robert W. Holt
Jennifer-Lynn H. Demers
Kristian J. Sexton
Jason R. Gunn
Scott C. Davis
Kimberley S. Samkoe
Brian W. Pogue

Tomography of epidermal growth factor receptor binding to fluorescent Affibody *in vivo* studied with magnetic resonance guided fluorescence recovery in varying orthotopic glioma sizes

Robert W. Holt,^{a,†} Jennifer-Lynn H. Demers,^{b,†} Kristian J. Sexton,^b Jason R. Gunn,^b Scott C. Davis,^b Kimberley S. Samkoe,^{b,c} and Brian W. Pogue^{a,b,c,*}

^aDartmouth College, Department of Physics & Astronomy, Hanover, New Hampshire 03755, United States

^bDartmouth College, Thayer School of Engineering, Hanover, New Hampshire 03755, United States

^cGeisel School of Medicine at Dartmouth, Department of Surgery, Hanover, New Hampshire 03755, United States

Abstract. The ability to image targeted tracer binding to epidermal growth factor receptor (EGFR) was studied *in vivo* in orthotopically grown glioma tumors of different sizes. The binding potential was quantified using a dual-tracer approach, which employs a fluorescently labeled peptide targeted to EGFR and a reference tracer with similar pharmacokinetic properties but no specific binding, to estimate the relative bound fraction from kinetic compartment modeling. The recovered values of binding potential did not vary significantly as a function of tumor size (1 to 33 mm³), suggesting that binding potential may be consistent in the U251 tumors regardless of size or stage after implantation. However, the fluorescence yield of the targeted fluorescent tracers in the tumor was affected significantly by tumor size, suggesting that dual-tracer imaging helps account for variations in absolute uptake, which plague single-tracer imaging techniques. *Ex vivo* analysis showed relatively high spatial heterogeneity in each tumor that cannot be resolved by tomographic techniques. Nonetheless, the dual-tracer tomographic technique is a powerful tool for longitudinal bulk estimation of receptor binding. © The Authors. Published by SPIE under a Creative Commons Attribution 3.0 Unported License. Distribution or reproduction of this work in whole or in part requires full attribution of the original publication, including its DOI. [DOI: [10.1117/1.JBO.20.2.026001](https://doi.org/10.1117/1.JBO.20.2.026001)]

Keywords: tomography; molecular; fluorescence molecular tomography; diffuse optical tomography; diffuse; reconstruction; magnetic resonance imaging.

Paper 140525R received Aug. 19, 2014; accepted for publication Dec. 23, 2014; published online Feb. 4, 2015.

1 Introduction

Fluorescence tomography of animals is inherently nonquantitative without employing significant system-specific calibration protocols, and even with these efforts, tracer delivery mechanisms confound recovery of specific tracer-to-receptor binding. Recently, a novel dual-tracer technique was introduced to overcome the problem of nonspecific uptake in molecular imaging and, thus, enable quantitative estimation of receptor concentration *in vivo*.¹⁻³ In this approach, two tracers are imaged simultaneously, one targeted to the receptor of interest and the other a nontargeted reference tracer. Comparing the uptake of these dyes enables recovery of binding potential, BP, a quantitative parameter proportional to the concentration of receptors available for binding.^{1,4-6} With the rise of targeted therapeutic agents in the treatment of cancer, BP is a potentially clinically relevant parameter, which can either inform in regards to the binding affinity of a new targeted drug to a model cancer tumor or be used for receptor concentration estimation of a tumor using a targeted drug of known affinity.

While the first orthotopic study to report on this technique reported dual-tracer tomography imaging,³ it did not examine the effect of tumor size on recovery of BP. As tumors grow, the feeding vessels and neovasculature growth and leakage

are extremely heterogeneous, and it is conceivable that within the regions of tumors the ability to quantify BP will be compromised by this. To examine this issue, the current study used image-guided fluorescence tomography (IGFT) to track BP of an orthotopic glioma tumor (U251 tumor line) over time as the tumors increased in size, using dual-tracer imaging.

In this study, the BP value for a receptor-targeted peptide was examined through *in vivo* and *ex vivo* imaging, tracking the values in a cohort of mice with tumors of varying sizes. The technique of directly measuring binding *in vivo* is relatively new, and the effect of tumor size on binding and receptor concentration remains largely untested. This study utilized an orthotopic glioma tumor line that overexpresses epidermal growth factor receptor (EGFR) in conjunction with a peptide, which has been designed to specifically bind this receptor. The variation with tumor size is hypothesized to alter vascular perfusion and permeability as well as obvious changes in the epidermal cell volume. A validation of the approach was sought by comparing *in vivo* measurement to *ex vivo* measurement.

2 Theory

It is possible to model the time-changing distribution of a tracer injected into a body if assumptions are made about the structural components that dominate the tracer flow inside the subject.⁷ An assumption is made that the temporal exchange is governed by linear exchange rates, k , and that the time changing concentrations in each compartment are driven by linear processes. Since these processes are largely convection and diffusion driven,

*Address all correspondence to: Brian W. Pogue, E-mail: brian.w.pogue@dartmouth.edu

[†]Authors contributed equally.

these assumptions are thought to be reasonably accurate when concentrations used are well below saturation levels. Thus, the concentrations of the targeted tracer dye in each compartment are governed by the following coupled ordinary differential equations:

$$\frac{dC_{B,T}}{dt} = k_3 C_{I,T} - k_4 C_{B,T}$$

$$\frac{dC_{I,T}}{dt} = K_1 C_{P,T} - (k_2 + k_3) C_{I,T} + k_4 C_{B,T}$$

$$\frac{dC_{P,T}}{dt} = K_1 C_{P,T} - k_2 C_{I,T}$$

For the second untargeted tracer, the equations are simpler:

$$\frac{dC_{I,UT}}{dt} = K_1 C_{P,UT} - k_2 C_{I,UT}$$

$$\frac{dC_{P,UT}}{dt} = K_1 C_{P,UT} - k_2 C_{I,UT}$$

where C_p is the concentration of dye in the blood/plasma, C_i is the concentration of the tracer in the interstitial fluid, and C_B is the targeted tracer, which is bound to the target of interest. Note that the secondary subscripts, T and UT, on the concentrations denote targeted dye and untargeted dye, respectively.

The first single targeted tracer compartment model cannot be solved without sufficient input data as it contains four unknown rate constants (K_1 to k_4). However, this problem can be overcome by incorporating an untargeted tracer with similar plasma pharmacokinetics as the targeted tracer such that the exchange rates with the blood concentration are the same for both dyes (i.e., K_1 and k_2 are the same for both dyes). Since these rates can often be determined using independent techniques, two dyes can be chosen which have comparable vascular permeability and plasma pharmacokinetic values. These values are largely determined by molecule size, charge, and lipophilicity, which are all known *a priori* and can be used to inform the selection of an appropriate reference tracer. It is also assumed that the number of target sites, which are available for the targeted tracer, are very large compared to the number of tracer molecules, meaning that the existence of targets does not

appreciably affect the blood or interstitial concentrations of the targeted dye. This is feasible in practice by simply injecting tracer doses such that the concentration in the tumor is much less than the receptor concentration, which is reasonable for tumors with high receptor expression. This can also be validated by ensuring that as higher doses are used the uptake does not saturate.

Under these assumptions, it is possible to use the untargeted tracer as a point of reference to isolate the effects of the targeted tracer binding to targets such that the differences in the uptakes of the two tracers will be due to the target binding. Essentially, the reference tracer accounts for the effects of nonspecific binding (i.e., the targeted tracer localizing where there are no targets), since the reference tracer will accumulate similarly. The underlying system of differential equations, relevant proofs, resulting solutions, and applications have been studied extensively⁷⁻¹¹ and, thus, will not be reproduced here. It is possible to linearize the convolution solution to these reference models under the above assumptions to produce a solution without convolution that is easily invertible.¹²

$$Q_T(t) = -\left(\frac{k_2}{1+BP}\right) \int_0^T dt Q_T(t) + k_2 \int_0^T dt Q_U(t) + \frac{K_1}{k_2} Q_U(t), \quad (1)$$

where Q_T is the measured bulk concentration of the targeted tracer (i.e., the local sum of all compartmental contributions), Q_U is the concentration of the untargeted tracer, and T is some final time. The concentrations Q_U and Q_T are typically measured using epi-illumination schemes, but can also be recovered tomographically. These represent observed or apparent bulk concentrations and are, thus, composed of a linear combination of the concentrations shown in Fig. 1. Using temporal measurements of the fluorescence concentrations recovered from IGFT, the above equation can be inverted to recover the kinetic parameters, including the BP defined as the ratio k_3/k_4 .

While tomographic techniques allow time-dependent imaging of the tracer pair, in cases not accessible to IGFT it is possible to approximate BP using a time-independent ratio at an instant in time, which is sometimes described as a snapshot method,² approximated as

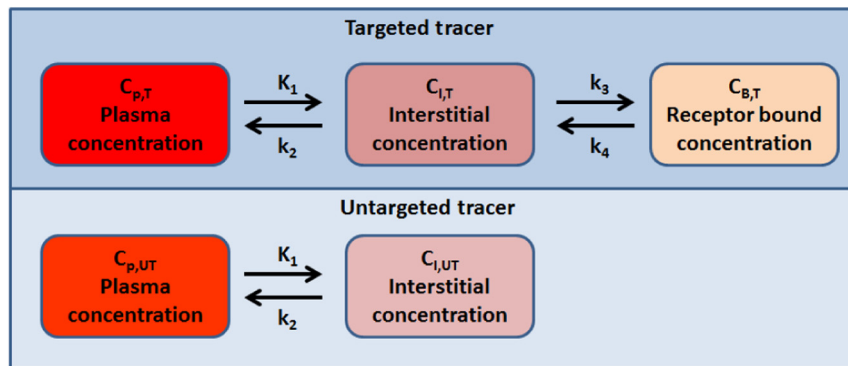


Fig. 1 A schematic diagram of the compartment model used to fit fluorescent tracer kinetics. The top targeted tracer reaches three compartments with four kinetic rate parameters, while the lower nontargeted tracer is chosen to have matched K_1 and k_2 parameters, but does not bind and, therefore, only requires two compartments. By combining the known values, the nontargeted tracer provides a reference, which can allow estimation of the k_3 and k_4 parameters for the targeted tracer. The ratio k_3/k_4 is known as the binding potential (BP) for that tracer to the receptor.

$$BP \approx \frac{Q_T - Q_U}{Q_U} \quad (2)$$

This snapshot method for BP maps is used in the *ex vivo* slice imaging section of this study to estimate the level of BP heterogeneity on the millimeter scale, which cannot be observed with diffuse tomography methods due to blurring of the light paths.

3 Methods

All animal studies were approved by the local Institutional Animal Care and Use Committee at Dartmouth College. A series of athymic mice ($n = 30$) were each implanted orthotopically with 1 million cells of a U251-green fluorescent protein (GFP) human glioma tumor line. This tumor line was chosen because it is known to overexpress EGFR, enabling specific targeting using an engineered peptide with high affinity for EGFR, the anti-EGFR targeted Affibody (Affibody, Sweden).^{3,13-15} Transfection of the cell line with GFP allows the GFP signal to be measured *ex vivo* and provides definitive tumor localization.¹⁶ The growth of the tumors was monitored using gadolinium-enhanced T1-weighted magnetic resonance imaging (MRI),

which was also the method used to gather anatomical prior information for fluorescence tomography. The general imaging scheme (as shown in Fig. 2) was to record MRI images, perform dual-tracer fluorescence tomographic imaging for up to 1 h, and then euthanize the animal for *ex vivo* analysis. The animal crania were partially frozen and then cut into thick sections for *ex vivo* planar fluorescence imaging, allowing spatially resolved quantification of fluorescence probe signal as well as GFP signal from the tumors. The animals were imaged in a staggered fashion, allowing the study of uptake and binding as a function of tumor size as tumor size is generally proportional to time post implantation. Animals were tomographically imaged on days 5, 8, 11, 14, 18, and 21 post tumor implantation. A dual-tracer method was used, with IRDye800CW (LI-COR Biosciences, Lincoln, Nebraska) conjugated to the anti-EGFR Affibody peptide serving as the targeted tracer. Conjugation procedures followed those described by Sexton et al.¹⁷ IRDye680RD (LI-COR) conjugated to a nonspecific Affibody peptide (Affibody negative control) was used as the reference tracer. The mice to be imaged were injected via tail vein with 0.1 nmol of each tracer and imaged continuously over the course of ~1 h, after which time each animal was sacrificed and then imaged *ex vivo*.

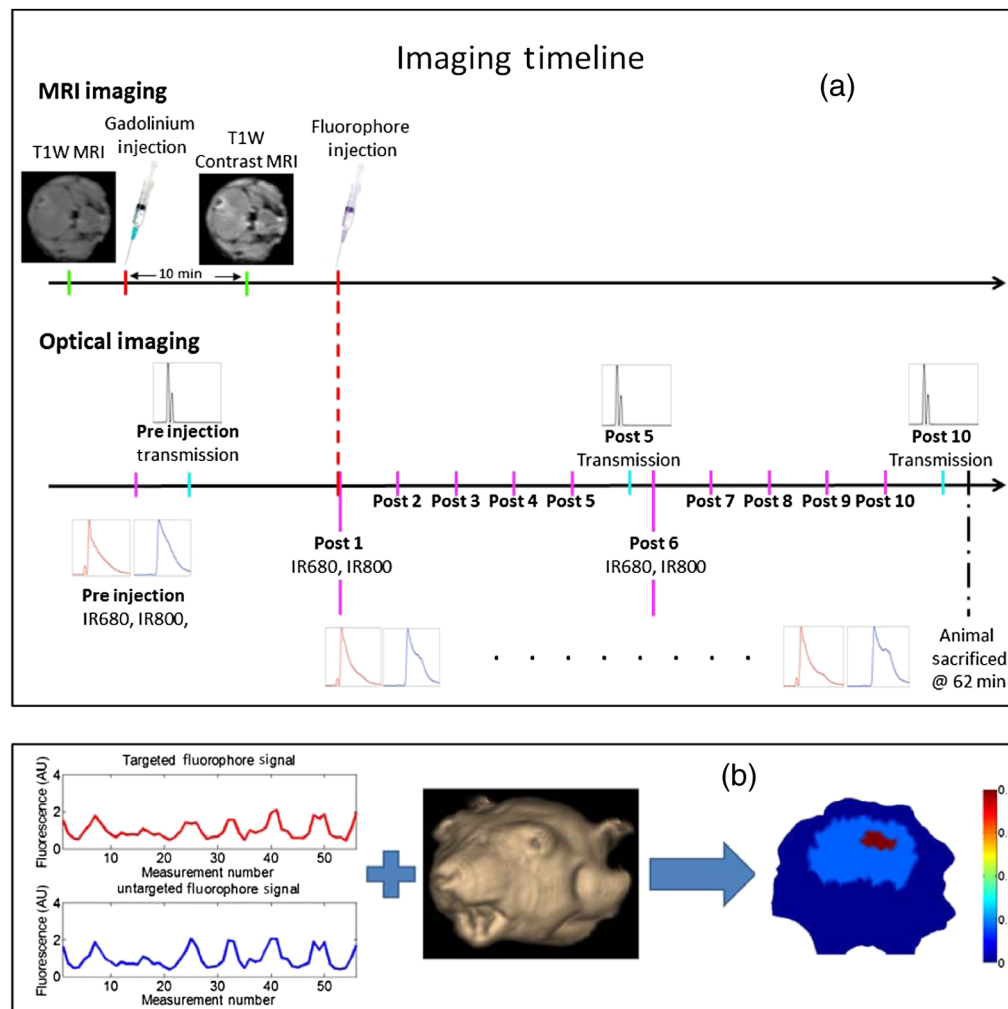


Fig. 2 (a) The imaging timeline of dual-tracer study is shown, with a tomographic data set acquired for each postinjection (post) imaging frame. The schematic diagram demonstrates the conceptual workflow from measurements to binding potential calculation. (b) Optical projection data are used in tandem with three-dimensional anatomical images of the head to recover anatomically guided binding potential maps.

The fluorescence tomography system used for imaging has been previously described,^{3,13} so only the salient details that differ from previous work will be discussed here. For IRDye800, the excitation was performed with a 690-nm diode laser providing 0.8 mW output at the tissue surface, and the necessary filtering on the emission side was accomplished using 720-nm low pass (LP) filters located inside a custom entrance optic for each of the eight spectrometers used for detection. IRDye680 excitation was performed with a 670-nm diode laser providing ~2 mW at the tissue, and filtering on the emission side was accomplished with 680-nm LP filters placed before each spectrometer. Each detection channel measured a spectral band of ~80 nm, and the intensity attributed to the IRDyes was found by spectral fitting of the fluorescence peak, which ensures accurate removal of the autofluorescence.¹³ Tissue phantom imaging using a mouse head geometry indicated that detection of fluorescence was feasible down to a level of at least 0.1 nM.

Optical measurements were made using eight fibers placed around the mouse's head. For each fiber-source and fiber-detector, the fluorescence through the head was acquired, as was the transmission of the excitation light through the head. For each source fiber, when the light was turned on, all detector fibers could readout the signal in parallel, due to having a separate spectrometer on each channel. Each source location was used to acquire signal for a maximum of 10 s, with both fluorescence and excitation scans done sequentially, using up to a maximum acquisition time of 160 s (8 sources \times 2 detection patterns \times 10 s each). The short optical scan time coupled with a longer MRI time allowed for the fiber locations to be monitored with MRI scans. This allowed adjustments to be made to the fiber positions to maximize optical probing at the tumor site. T1-weighted MR scans also provided the spatial information needed to generate three-dimensional (3-D) meshes of the mouse head. Gadolinium contrast scans (200 μ L gadolinium injections per mouse) were used to determine the extent of the tumor and to aid in segmentation (Magnevist, Bayer HealthCare, Whippany, New Jersey).

Dual source detection is sequentially implemented by having the two previously mentioned diode lasers cycle into the source location through manual switching while a filter wheel at each spectrometer rotates to the corresponding cut on filters. The 670-nm laser was used in conjunction with 680-nm LP filters in order to spectrally isolate the IRDye680-labeled compound, and then the 690-nm laser was used with the 720-nm LP filters for the IRDye800-labeled compound. The source was rotated to each fiber in an automated manner, and the filter wheels were stationary for each set of source rotations. The full spectrum emission at each detector was recorded for processing.

For each imaging frame, the collected fluorescence data were spectrally processed and Born-normalized. The eight-fiber fluorescence imaging system did not permit simultaneous excitation and intensity collection in a single channel, resulting in 56 optical projection measurements per frame for 10 temporal frames. Segmentation based on the anatomical structural information was performed using the NIRView software package.^{18,19} A 3-D finite element method mesh was then produced for each mouse.³ Each mesh was assigned three regions: tumor, nontumor brain, and bulk tissue. A uniform region-based recovery was performed for each frame. BP was calculated for every target site from the resulting time-course fluorescence recovery [Fig. 2(a)]. In addition, BP fitting was performed on the single optical projection which most appreciably probed the tumor.

Following imaging and sacrifice, animals were frozen at -20°C and the head was later sectioned into slices of ~2 mm thickness using a custom cryoslicing instrument. These slices were then imaged for GFP as well as IRDye 680RD and IRDye 800CW. The GFP signal was used to confirm the size and location of the tumor (Typhoon FLA scanner, GE Healthcare Life Sciences) and IRDye 680RD and IRDye 800CW were imaged to enable localization of tracers (Pearl Imager, LI-COR Biosciences).

4 Results

Examples of the GFP images taken from frozen sliced cranium of 12 mice are shown in Fig. 3, clearly illustrating the variations in tumor size. Note that these images are in negative contrast, so that high fluorescence is seen as darker in the image. Figure 3 also shows the tumor sizes derived from contrast MRI scans by segmenting each 3-D volume, during the mesh creation process. As expected, the growth rate of the tumor can be modeled exponentially, and a fit to the data matches $V(t) = 0.13 \text{ mm}^3 * \exp(0.25 * t)$, where V is the volume in cubic millimeters and t is the time after tumor implantation in days. This average data fit curve indicates a characteristic growth time of 0.25 d^{-1} , or a doubling time of 2.77 days.

Figure 4 (top) shows a comparison between the tomographically recovered BP values of the mice versus direct temporal curve fitting of the source-detector pair, which maximally sampled the tumor location. Tumors whose sampling sensitivity was below a threshold of 5% of the total were removed from the plot, as the BP fits would then be erroneously low. This would not be due to true BP variation, but rather from partial volume averaging error where normal brain dominated the signal. The data were also plotted as a function of tumor size, in the middle graph of Fig. 4, where there is no apparent trend. This indicates that there was no discernable effect of tumor size upon the recovered BP values. In the bottom plot of Fig. 4, the raw

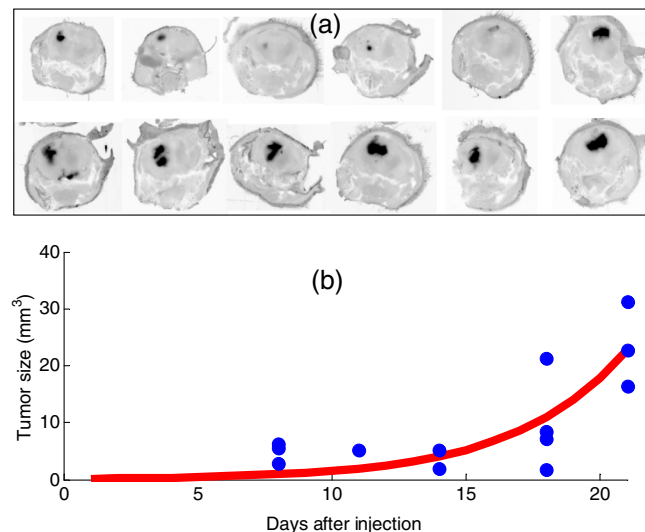


Fig. 3 (a) Fluorescence images of green fluorescent protein (GFP) distribution within cryosectioned cranium samples are shown for 12 mice, showing the range of tumor sizes in the study. (b) The tumor volume over time was estimated by magnetic resonance imaging scans and is shown for each of the mice imaged, illustrating the expected average orthotopic glioma tumor growth curve with time after implantation for this cell line.

fluorescence value is plotted against tumor volume, showing that the smaller tumors have both higher variance and overall higher average fluorescence than the larger tumors.

Figure 5 shows a characteristic series of *ex vivo* slice images by epi-illumination fluorescence imaging, of the IRDye 680RD and IRDye 800CW. These images were used to estimate the BP map by simple subtraction and ratioing, as outlined above. The GFP image showing the tumor is also shown in the bottom row, with the resulting segmentation based on this image shown next to it. Interestingly, the GFP area is clearly different from the BP enhanced area in the brain, indicating that heterogeneity of binding exists within the tumor region. This slight mismatch

between the peaks in BP and GFP expression was observed in most tumors where there was no identical overlap between the BP images and the GFP images. It is also important to point out that the BP estimate images shown in Fig. 5 were derived from epi-illumination images which were not spectrally fit, as was done in the tomography system. The epi-illumination system used in this study had a single filter setting at each emission, so there is potential for the BP *ex vivo* images to not be exactly matched to the GFP images due to autofluorescence or background fluorescence contamination. The data were interpreted quantitatively in Fig. 4 (top), which shows bulk average values for the entire tumor.

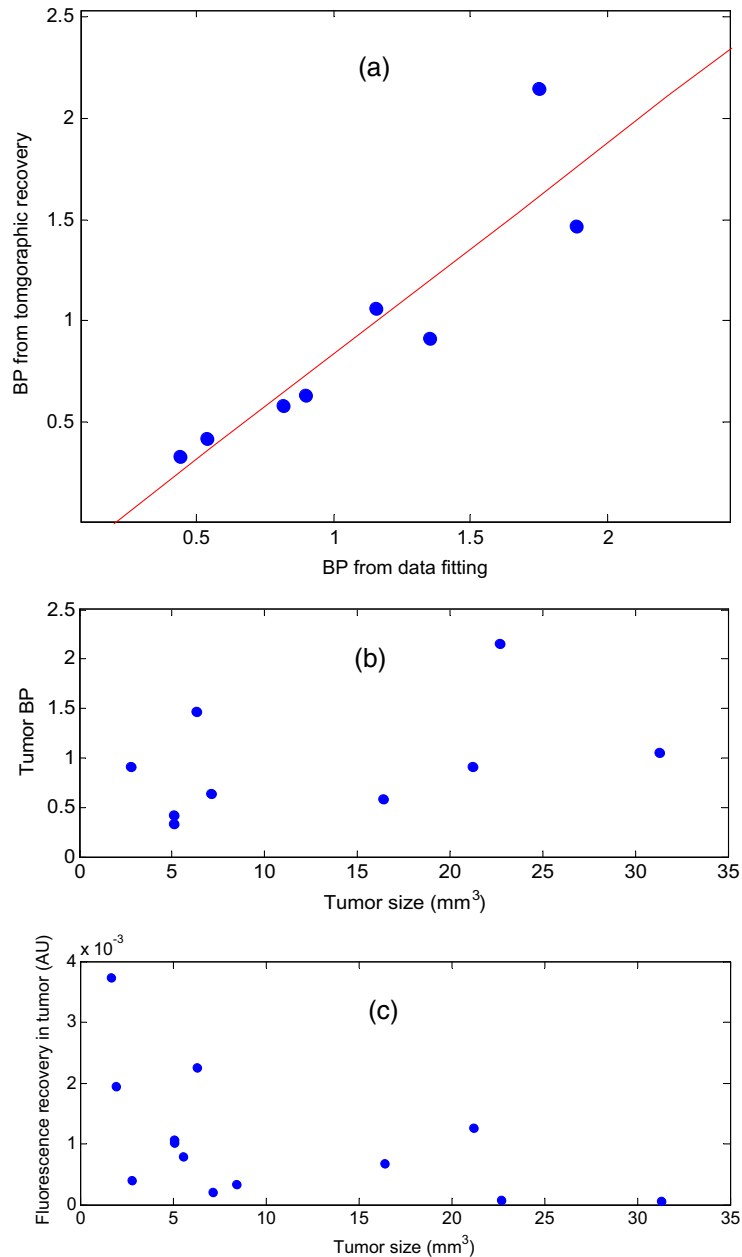


Fig. 4 (a) A comparison of BP values recovered from postprocessing of tomographic image recovery (vertical axis) compared to the BP values estimated by processing the raw tomographic data from a single set of source–detector pairs, which optimally probed the tumor site. The line of best fit is also shown for these data. (b) A comparison of the tomographically recovered tumor BP values versus tumor volume. There is no significance to linear fitting of these data, indicating no clear trend is present between BP value and tumor size. (c) The raw fluorescence values are plotted against tumor size.

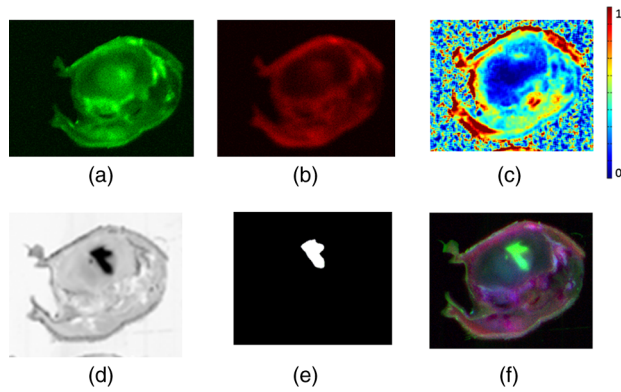


Fig. 5 A single cross-sectional slice of the entire mouse head is shown with brain region in the upper mid-half. (a) Characteristic untargeted tracer slice image. (b) Characteristic targeted tracer slice image. (c) Binding potential image resulting from snapshot processing of (a) and (b). (d) Green fluorescent protein highlighting image. (e) Segmentation of tumor site from GFP image. (f) RGB overlay with the targeted image in the red channel, the GFP image in the green channel, and the untargeted image in the blue channel.

5 Discussion

The overall goal of this work was to utilize a dual-tracer tomography system to image EGFR expression in orthotopic glioma tumors at various stages of growth. A previous study examined BP imaging using fluorescence tomography in a limited number of animals,³ but the method has not been validated in a range of tumors with varying size. The particular importance of this is that, while it is known that permeability conditions and vascular perfusion conditions change considerably as tumor size changes, it is unknown how these changes affect the availability of target receptors.

The binding potential values recovered in this study reflect comparable values found elsewhere for the U251 tumor line.^{3,9} Importantly, we observed that the recovered values of binding potential were not a function of tumor size, indicating that the vascular and cellular stage of the tumor does not have a measurable effect upon the observed bulk receptor density. This suggests that receptor imaging can be a valuable tool because the receptor density is a distinct property of an individual tumor. Consequently, animals can be studied at a range of tumor growth stages for receptor density.

The MRI images were inspected to ensure the optical system sufficiently probed the tumor, as the tomographic fiber array was occasionally positioned with poor coverage of the tumor. The MRI images were used to simulate forward data to determine tumor sensitivity and only animals for which 5% of the summed optical sensitivity was found in the tumor were included in the analysis.

Single source–detector projections through the tumor were identified using the associated MR images and were also used to assess BP. These values correlated with the values in the tumor recovered using full tomographic imaging (Fig. 4, top), suggesting that, in some cases, full tomographic imaging may not be necessary to recover bulk values of BP in the tumor. Interestingly, it is clear from the other data in Fig. 4 (lower graph) that the raw fluorescence value does not report on the volume of the tumor at all, and in this data set, there was actually an inverse relationship between tumor size and fluorescence. The nature of this inverse relationship is not fully known, although it could be due to increasing regions of necrosis in

the tumors and the corresponding partial volume artifacts due to region-based fluorescence recovery.

The distribution of the two tracers in the planar images is far from ideal for tumor localization, although clearly visible above the level in the normal brain, and was validated by *ex vivo* imaging studies. Skin is well known to express large amounts of EGFR, so the whole head slices show this signal is strongly present in the surrounding skin. The processed BP images, although somewhat noisy, provide a clear localization of the binding in the brain tumor, which would not be apparent by simply inspecting the individual images from either the targeted or nontargeted images.

The use of the dual-tracer technique to examine the tumor site can help guide treatment since it potentially correlates to an appropriate dose of targeted drug and can be used to confirm whether the drug is binding in the tumor. This technique has particular relevance to assessing the value of new targeted therapeutics in drug discovery studies. Alternatively, if this type of imaging is done on individual subjects, it could be feasible to determine or track the efficacy of a targeted therapeutic at each individual tumor site.

6 Conclusion

The ability of dual-tracer methods to quantify BP values in a range of tumor sizes *in vivo* was examined in this work. It was shown that in the orthotopic U251 tumor line, the binding potential appears to be invariant with tumor size for the range of sizes examined. This stability may prove an important observation for the dosing or monitoring of receptor-targeted therapies. It was also shown that directly sampled optical projections across the tumor regions might be as valuable for assessing BP as full tomographic recovery. This is an important verification originally observed in single molecule imaging,¹⁴ which could greatly simplify the data acquisition and analysis for BP studies. It should be reiterated that this conclusion was tested only in a single tumor line, the orthotopic U251 glioma, and should be tested in other tumor lines before a more global statement can be made about the consistency of BP values across tumor sizes.

Acknowledgments

This work was funded by NIH grants R01 CA109558, R01 CA167413, and R01 CA184354.

References

1. K. M. Tichauer et al., "Advantages of a dual-tracer model over reference tissue models for binding potential measurement in tumors," *Phys. Med. Biol.* **57**(20), 6647–6659 (2012).
2. K. M. Tichauer et al., "Improved tumor contrast achieved by single time point dual-reporter fluorescence imaging," *J. Biomed. Opt.* **17**(6), 066001 (2012).
3. S. C. Davis et al., "Dynamic dual-tracer MRI-guided fluorescence tomography to quantify receptor density *in vivo*," *Proc. Natl. Acad. Sci. U S A* **110**(22), 9025–9030 (2013).
4. K. M. Tichauer et al., "Dual-tracer background subtraction approach for fluorescent molecular tomography," *J. Biomed. Opt.* **18**(1), 016003 (2013).
5. M. A. Mintun et al., "A quantitative model for the *in vivo* assessment of drug binding sites with positron emission tomography," *Ann. Neurol.* **15**(3), 217–227 (1984).
6. M. Laruelle, M. Slifstein, and Y. Huang, "Positron emission tomography: imaging and quantification of neurotransmitter availability," *Methods* **27**(3), 287–299 (2002).

7. A. A. Lammertsma and S. P. Hume, "Simplified reference tissue model for PET receptor studies," *Neuroimage* **4**(3), 153–158 (1996).
8. R. B. Innis et al., "Consensus nomenclature for *in vivo* imaging of reversibly binding radioligands," *J. Cereb. Blood Flow Metab.* **27**(9), 1533–1539 (2007).
9. K. M. Tichauer et al., "In vivo quantification of tumor receptor binding potential with dual-reporter molecular imaging," *Mol. Imaging Biol.* **14**(5), 584–592 (2012).
10. K. S. Samkoe et al., "High vascular delivery of EGF, but low receptor binding rate is observed in AsPC-1 tumors as compared to normal pancreas," *Mol. Imaging Biol.* **14**(4), 472–479 (2012).
11. A. K. Liu, M. E. Macy, and N. K. Foreman, "Bevacizumab as therapy for radiation necrosis in four children with pontine gliomas," *Int. J. Radiat. Oncol. Biol. Phys.* **75**(4), 1148–1154 (2009).
12. M. Ichise et al., "Strategies to improve neuroreceptor parameter estimation by linear regression analysis," *J. Cereb. Blood Flow Metab.* **22**(10), 1271–1281 (2002).
13. S. C. Davis et al., "Magnetic resonance-coupled fluorescence tomography scanner for molecular imaging of tissue," *Rev. Sci. Instrum.* **79**(6), 064302 (2008).
14. S. C. Davis et al., "Comparing implementations of magnetic-resonance-guided fluorescence molecular tomography for diagnostic classification of brain tumors," *J. Biomed. Opt.* **15**(5), 051602 (2010).
15. K. M. Tichauer et al., "Computed tomography-guided time-domain diffuse fluorescence tomography in small animals for localization of cancer biomarkers," *J. Vis. Exp.* **17**(65), e4050 (2012).
16. K. S. Samkoe et al., "Protoporphyrin IX fluorescence contrast in invasive glioblastomas is linearly correlated with Gd enhanced MR image contrast but has higher positive predictive value," *J. Biomed. Opt.* **16**(9), 096008 (2011).
17. K. Sexton et al., "Fluorescent Affibody peptide penetration in glioma margin is superior to full antibody," *PLoS One* **8**(4), e60390 (2013).
18. M. Jermyn et al., "Fast segmentation and high-quality three-dimensional volume mesh creation from medical images for diffuse optical tomography," *J. Biomed. Opt.* **18**(8), 086007 (2013).
19. www.nirfast.org.

Robert W. Holt graduated in 2014 with a PhD in physics and astronomy from Dartmouth College, where he was awarded the institution's Hannah Croasdale Award for academic excellence. His research interests include innovative multimodal image synthesis and novel image analysis methods development. He works as an image analysis developer for inviCRO, LLC, in Boston, Massachusetts.

Jennifer-Lynn H. Demers recently graduated with a PhD in engineering science from Dartmouth College. Her research is in the area of optical tomography methods and comparative imaging using luminescence, fluorescence, Raman, and surface-enhanced Raman spectroscopy.

Kristian J. Sexton recently graduated with a PhD in engineering science from Dartmouth College. His research is in the area of optical tools for surgical guidance and tissue diagnostics. He is currently a research fellow at the Institute of Photonics Sciences in Barcelona, Spain.

Jason R. Gunn is the Lifescience manager of the Optics in Medicine Laboratory at Dartmouth, funded through the Thayer School of Engineering and housed within the Surgical Research Labs at the Dartmouth-Hitchcock Medical Center. His expertise is in laboratory methods for therapeutic and imaging evaluation for pancreatic cancer, glioblastoma, and xenograft models.

Scott C. Davis, PhD, is an assistant professor of engineering at Dartmouth College and holds degrees in physics, mechanical engineering, and biomedical engineering. His research aims to develop and assess new optical imaging technologies to diagnose tissue and guide cancer therapy. He currently directs a National Cancer Institute-funded research project to develop multi-tracer deep-tissue optical imaging techniques to quantify molecular biomarkers *in vivo*. He has published over 40 peer-reviewed articles covering multimodal optical imaging, fluorescence spectroscopy and imaging for surgical guidance, and dosimetry of PDT and radiation therapy.

Kimberley S. Samkoe is a research assistant professor in the Department of Surgery at Geisel School of Medicine and an adjunct assistant professor at Thayer School of Engineering at Dartmouth College. She obtained her PhD in biophysical chemistry from the Department of Chemistry at the University of Calgary, Alberta, Canada, in 2007. Her current research involves fluorescence imaging of targeted agents for cancer diagnosis and therapeutic monitoring, as well as photodynamic therapy.

Brian W. Pogue is professor of engineering, physics and astronomy, and surgery at Dartmouth College in Hanover, New Hampshire, USA. He has a PhD in medical/nuclear physics from McMaster University, Canada. He works in the area of optics in medicine, with a focus on novel imaging systems for characterizing cancer and imaging therapy. He has published over 230 peer-reviewed papers in the areas of biomedical optics, and his research is funded by the National Cancer Institute.